Self-assembled silver-germanium metasurfaces with the enhanced nonlinear response

Authors: T. Stefaniuk[1]*, N. Olivier[1], A. Belardini[2], C. McPolin[1], C. Sibilia[2], A. A. Wronkowska[3], A. Wronkowski[3], T. Szoplik[4], A. V. Zayats[1]

Affiliations:

[1]Department of Physics, King's College London, Strand, London, WC2R 2LS, UK

[2]Department of Basic and Applied Science for Engineering, Sapienza Università di Roma, Via Antonio Scarpa, 16, 00161 Roma, Italy

[3]Institute of Mathematics and Physics, UTP University of Science and Technology, Kaliskiego 7, 85-796 Bydgoszcz, Poland

[4]Faculty of Physics, University of Warsaw, Pasteura 7, 02-093 Warsaw, Poland

*Correspondence to: tomasz.stefaniuk@kcl.ac.uk

Introductory paragraph: The concept of metamaterials and metasurfaces opened an avenue for designing and fabricating functional optical devices with unique linear and nonlinear optical properties, relying on geometrical arrangement of nanostructures[1]. Metamaterials have been successfully used to achieve negative refraction[2], controlling density of optical states and spontaneous emission[3, 4], artificial magnetism[5], the enhanced nonlinear properties[6, 7], as well as flat lenses[8, 9] and holograms[10, 11]. Here we show that a nanostructured metasurface can be spontaneously formed near an interface of a thin film of silver. Interplay between a grain boundary structure and surface segregation of Ge atoms in Ag films leads to encapsulation of the grains and, as a result, formation of a nanoparticle composite near the film surface. The resulting composite Ag/Ge surfaces exhibit strong localized surface plasmon resonances leading to extraordinary second harmonic generation for both p and s polarized light with up to 2 orders of magnitude enhancement compared to Ag thin film without Ge. Segregation phenomena open the possibility for fabrication of a new class of composite materials and gives additional degree of freedom in designing optical properties of nanostructured metamaterials.

Main Text:

In recent years the nonlinear properties of plasmonic metamaterials have been intensively exploited. Metals provide some of the highest and fastest nonlinearities compared to semiconducting or transparent dielectrics due to strong local field enhancement, complex electron dynamics and overall design of the structure which might improve the inherent nonlinear optical behavior[12]. Strong Kerr type optical nonlinearity, at the wavelengths where negligible nonlinearity of the consistent materials exist[7] as well as second- and higher-order harmonic responses were investigated theoretically[13, 14] and experimentally[15, 16]. While it has been proven that metamaterial structure can enhance harmonic generation, the centrosymmetry of metals implies that interface induced break of symmetry is necessary for generation of even-order harmonics. As a result, only polarization component perpendicular to the surface of metals can efficiently participate in frequency doubling[17, 18] resulting in a strong polarization dependence of second-harmonic generation (SHG), only allowed for p-polarized excitation light from a smooth surface. While roughness results in relaxation of this rule, overall, the s-polarized excitation of SHG is much weaker from centrosymmetric metals.

There are two main approaches for metamaterials fabrication based on top-down nanostructuring and bottom-up self-assembly. The former uses traditional micro- and nano-fabrication methods to form materials from composites desired shapes and order[8]. In the latter, structuring is achieved by a self-organization process which is controlled by various strategies[19, 20, 21, 22]. One of such self-organization processes, called segregation, leads to separation of admixture atoms in small regions within the matrix medium, defined by the presence of inhomogeneities in the matrix, such as free surfaces, grain boundaries, interfaces between different phases or dislocations[23]. Among these types, a particularly interesting one is segregation at the

grain boundaries, which is driven by the reduction of the grain boundary energy. Although its range is limited to the nanometer scale, it can reach much larger concentration differences than other types of segregation[24]. One of the pairs of materials which exhibit segregation is silver and germanium[25]. This combination was rediscovered for plasmonic applications when 1-2 nm thin Ge wetting films were proposed to overcome silver tendency to form clusters rather than smooth layers[26, 27, 28]. However, it has been recently shown that the penetration of Ge atoms along high-diffusivity paths in silver not only changes the resistivity of silver thin films[29], but also has a significant impact on their optical properties[30].

Here we use the segregation mechanism to form Ag/Ge metasurface with unique nonlinear optical properties. We show that apart from the localized surface plasmon (LSP) resonances exited due to surface roughness, this system exhibits LSPs originating from encapsulated silver grains, which has much stronger influence on the linear optical properties of the thin Ag/Ge films. The segregation process breaks the centrosymmetry of silver host, leading to generation of SH for p- and, extraordinary, for s-polarized excitation light with up to 2 orders of magnitude enhancement compared to smooth Ag films without Ge.

The studied Ag/Ge metasurface (Fig. 1A) was formed by Ge diffusion and segregation near the Ag-air interface (see Methods for the details of fabrication). The presence of the 1 nm amorphous Ge wetting layer during the e-beam evaporation process of Ag changes the kinetics of growth of Ag and smoothens even a 100 nm thick silver film. The average diffusion length of Ag adatoms is significantly shorter on Ge than on SiO_2 substrate, resulting in a more compact silver film with smaller grain sizes[31, 32]. The Ag/Ge sample has a more uniform distribution of nanocrystals at the surface and lacks large crystallites, compared to Ag film (Fig. 1B).

The weak absorption resonances observed for a pure Ag film near a wavelength of 360 nm (Fig. 1c) can be associated with LSP excitations due to the roughness of the film[30]. They disappear for a smoother Ag/Ge metasurface. The reflection spectra of the Ag/Ge metasurface reveal a strong absorption resonance at around 640 nm wavelength, absent in Ag film without Ge, whose origin can be traced to LSPs of Ge-encapsulated silver grains. This peak increases with time together with DC resistivity and can be attributed to segregation of Ge atoms from the wetting layer towards the surface of Ag film, as observed in *ex-situ* XPS measurements. This process evolves in time and 14 days after the evaporation, only a fraction of the original amount of Ge atoms remains on Ag-substrate interface[30] and most of the Ge atoms segregate to Ag free surface, which can be considered as largest defect in the structure, and into silver grain boundaries near the Ag-air interface. For comparison, when a 1 nm thick Ge layer is evaporated on top of a pure silver, the reflection spectrum no longer exhibits the resonance related to the encapsulation of the silver grains in Ag/Ge composite. Since the film surface has the lowest Gibbs energy, Ge atoms no longer have a tendency to segregate inside the Ag film and to form a composite. If a Ag/Ge metasurface is additionally covered with a 10 nm thick layer of amorphous SiO_2, the features of the reflection spectrum related to LSPs due to both the roughness and encapsulated Ag/Ge grains are observed. The latter one is however suppressed since the presence of fused silica limits the segregation of Ge to the SiO_2/Ag interface as the surface states are already occupied by SiO_2 atoms. Silica layer also leads to a shift of both LSP resonances due to the changes of refractive indexes of the adjacent medium, as expected for LSP modes (see Supplementary Information for more details).

The optical properties of the Ag/Ge grain composite near the surface of the film were modelled assuming that in equilibrium the silver grains are encapsulated by Ge atoms that breaks the electrical connection between the grains[29]. This may occur if at the beginning the Ge atoms

segregate to low-coordination-number surface states and only when they are occupied they stay in high-coordination-number Ag grain boundary states. The simulated reflection spectra (Fig. 1d) and the corresponding intensity distributions (Figs. 2a and b) describe the experimental data well for both rough Ag film and smooth Ag/Ge composite. The rough Ag film, modelled with grains of 30 nm size near the interface with air, exhibits a LSP at 356 nm wavelength and the incident electromagnetic field is concentrated near the surface of the film. In the case of Ag/Ge metasurface, the absorption maximum is near a wavelength of 640 nm corresponding to the LSP on the Ge-encapsulated, isolated silver grains of 20 nm size. In this situation the field is strongly concentrated below the surface around the grains. The metal between the grains in the composite, prevents electromagnetic interaction between the grains and, thus, the optical properties are determined by the behavior of individual grains. For the 2 other geometries considered in the experiment with Ge on top of a Ag film and with a silica protective layer, the numerical model confirms that without the presence of germanium at the boundary sites, the LSP resonance indeed does not exist, while a silica layer shifts the LSPs of the Ag/Ge composite due to its refractive index, as long as the amount of Ge atoms between the grains is enough to sever the electrical connection.

The grain structure of the composite near the Ag-air interface and the associated resonant field enhancement have profound impact also on the nonlinear optical properties (Fig. 3). The observed SHG from the Ag film (solid lines) is much stronger under excitation with p-polarized light, which should be expected for relatively smooth continuous metal surfaces[33]. Only the component of the electric field normal to the metal surface has a discontinuity at the boundary and gives rise to a dipole-allowed surface nonlinearity[34]. The decrease in the SH intensity near the interband transitions (around a wavelength of 310 nm) is also known and results from the interplay between free-electron plasma and core electrons in metals[35].

The second-harmonic spectra from the Ag/Ge metasurface are significantly different (Figs. 3a, b). Although, the presence of Ge atoms introduces extra losses, and, thus, the SH signal is weaker, near the LSP resonance excited on encapsulated grains, the situation dramatically changes. For p-polarized light, the generated SH signal at a wavelength of 325 nm is almost 20 times stronger than from the Ag surface under the same illumination conditions and despite the vicinity of the interband transitions, the intensity is almost 40% stronger than the highest SH intensity for all the measured wavelengths (Figs. 3c). Surprisingly, the SH signal enhancement is also observed for s-polarized light in the same spectral range. Not only does the enhancement factor at the LSP resonance exceeds 300, but the SH intensity is now of the same order of magnitude as the intensity observed under p-polarized illumination in metamaterial and much stronger than from a pure Ag surface. The wavelength dependence of SH intensity enhancement follows the behavior of the imaginary part of the effective permittivity of Ag/Ge (Fig. 3d).

Different efficiencies of the SH generation at the metasurface for p- and s-polarizations compared to a Ag surface can be explained in terms of the LSP field enhancement near the surface of a film, which is 2 times stronger for p polarization (Fig. 2) and symmetry breaking introduced by the encapsulated Ag grains (Fig. 2 and Supplementary Fig. 2). The grain encapsulation increases effective surface area needed for second-order nonlinear response. As a result, not only does the component of the electric field normal to the air-metal interface (E_z) participate in the frequency doubling, but so do the other components (E_x and E_y), which are usually not active in SHG process at a smooth metal interface, as they now, efficiently generate SH light from the grain boundaries below the air-metal interface.

We have demonstrated that the segregation mechanism leads to the formation of a metasurface which exhibits enhanced and polarization independent SHG. This unique process

breaks nonlinear optics paradigms of polarization selection rules of a dipole-allowed surface nonlinearity in centrosymmetric media. The spontaneously formed encapsulated grains near the surface determine both the polarization and wavelength dependent SH efficiency via their localized surface plasmon resonances. We show that strong frequency doubling can be achieved even at wavelengths where the interband transitions significantly reduce the nonlinear response of the metal, with up to 2 orders of magnitude enhancement compared to a rough Ag film. These results demonstrate the potential of a new class of composite metamaterials which can be formed using segregation processes and can be achieved in many plasmonic metals[24]. Bottom-up segregation process together with additional top-down nanostructuring may lead to 2-level hierarchical metamaterials and metasurfaces with the extended range of linear and nonlinear functionalities which are difficult to achieve in conventional metamaterials due to constituent material constraints.

Materials and Methods

Sample fabrication and physical characterization. Thin films were deposited using an electron-beam evaporator (PVD75, Lesker). During the evaporation process, the pressure in the chamber was 2×10^{-6} Torr and the sample holder was kept at room temperature. Single-sided polished fused silica glass substrates with nominal roughness rms $\leq$ 0.3 nm, were cleaned for 30 s with argon ions having 105 eV energy and a 0.2 mA/ cm^2 beam density before the deposition of layers. Ge films of 1 nm thickness were evaporated at the rate of 0.5 Å/s, Ag layers of 100 nm thickness at the rate of 10 Å/s and 10 nm thick SiO_2 overlayer at the rate of 1 Å/s. Subsequent layers were sequentially evaporated without breaking the vacuum. Film thicknesses were monitored using the oscillating quartz crystal. Atomic force microscope (Ntegra NT-MDT) measurements under tapping mode in air were carried to estimate the quality of the evaporated

surfaces. Before characterization, the samples were kept in ambient conditions in an Ar atmosphere. The averaged RMS values from AFM scans are 1.8±0.3 for Ag/Ge samples and 3.74±0.4 nm for Ag films. The SEM images of the samples were taken using the Zeiss Sigma microscope with acceleration voltage of 20 kV (Figs. 1a and b). We also investigated the interior structure of samples using one-dimensional wide-angle X-ray diffraction (Bruker GADDS system equipped with 2D Vantec 2000 detector). The averaged grain size of the Ag/Ge metasurface was approximately of 20 nm, and this diameter is considered in numerical simulation. The skin-depth of Ag is 12 nm at around 640 nm wavelength which is comparable to the size of the encapsulated grains. The grain size of the pure Ag reference film varies between 30 nm and 50 nm, depending on a particular area of the sample.

Linear optical characterization. Reflectance (Fig. 1c) and ellipsometry (Fig. 2d) measurements were performed in air using a rotating analyzer ellipsometer in the spectral range from 300 to 1000 nm (V-VASE, J.A. Woollam Co., Inc.). Ellipsometric parameters Ψ and Δ were determined for angles of incidence in the range $40° \leq \varphi \leq 80°$. Optical constants of the samples were calculated from the measured quantities using a regression procedure and the parametrization of optical functions model to match the experimental data.

Nonlinear spectroscopy. An amplified Yb:KGW femtosecond laser (Pharos, Light Conversion) together with an optical parametric amplifier (Orpheus, Light Conversion) were used to achieve light pulses in the wavelength range of 650-850 nm. 150 fs pulses with 100 kHz repetition rate were sent through a range of optical components (Supplementary Fig. 1) to control of polarization, power, divergence, and size of the beam. The peak power focused at the sample

surface using an Olympus LMPLN10XIR objective was of the order of 70 GW/cm^2 and the sample position was adjusted for every illumination wavelength. The residues of the fundamental incident beam were filtered out using band-pass filters (Thorlabs). The SH spectra were collected using spectrometer (IsoPlane SCT320, Princeton Instruments) equipped with a UV camera (ProEM:eXcelon3, Princeton Instruments) and were corrected to the transmission properties of the filters and objectives in the setup. The enhancement factor is defined as a ratio between SH signal intensity measured for Ag/Ge metasurface and pure Ag reference sample (Fig. 3). The optical characterization was performed 4 months after the evaporation of the samples.

Numerical modelling. To understand the nature of the metasurface resonance, a Finite Difference Time Domain modelling (Lumerical FDTD solutions) of the structure was performed taking into account the internal grain structure of the Ag/Ge film. We assumed that at the beginning the Ge atoms segregate to low-coordination surface states and only when they are occupied they stay in high-coordination Ag grain boundary states. As a result, in the equilibrium the silver grains are being encapsulated by Ge-type thin layer which breaks the electrical connection between the grains[29]. On the basis of these hypothesis, we retrieved reflection curves (Fig 1d) and the corresponding field intensity distributions (Figs. 3a and b). The sizes of the grains are estimated on the basis of X-ray diffraction measurements and are equal 20 nm for Ag/Ge composite and 30 nm for Ag reference sample. The separation of the grains equals 45 nm. The effective refractive index of the Ge nanoshell is $n_{Ag/Ge}$=1.1+0.1i and the 1.5 nm shell thickness is assumed. Although we use a relatively simple model to describe the complex geometrical structure of the composite material, the simulations for both the pure silver film and the metasurface provide good agreement with the measured data. The estimated shell refractive

index is between the refractive index of 100 nm thick Ag reference sample (n_{Ag}=0.064+4.285i) and 1 nm thick amorphous layer of germanium (n_{Ge}=3.33+0.24i), measured for 645 nm wavelength in our experiments. The refractive index of SiO_2 cover layer equals n_{SiO2}=1.462 + 0i for the same frequency.

References and Notes:

1. Shelby RA, Smith DR, Schultz S. Experimental verification of a negative index of refraction. *Science* 2001, **292**(5514)**:** 77-79.

2. Soukoulis CM, Linden S, Wegener M. Negative Refractive Index at Optical Wavelengths. *Science* 2007, **315**(5808)**:** 47-49.

3. Noginov MA, Li H, Barnakov YA, Dryden D, Nataraj G, Zhu G, *et al.* Controlling spontaneous emission with metamaterials. *Opt Lett* 2010, **35**(11)**:** 1863-1865.

4. Li J, Krasavin AV, Webster L, Segovia P, Zayats AV, Richards D. Spectral variation of fluorescence lifetime near single metal nanoparticles. *Scientific Reports* 2016, **5**.

5. Yen TJ, Padilla WJ, Fang N, Vier DC, Smith DR, Pendry JB, *et al.* Terahertz Magnetic Response from Artificial Materials. *Science* 2004, **303**(5663)**:** 1494-1496.

6. Wurtz GA, Pollard R, Hendren W, Wiederrecht GP, Gosztola DJ, Podolskiy VA, *et al.* Designed ultrafast optical nonlinearity in a plasmonic nanorod metamaterial enhanced by nonlocality. *Nature Nanotechnology* 2011, **6**(2)**:** 107-111.

7. Neira AD, Olivier N, Nasir ME, Dickson W, Wurtz GA, Zayats AV. Eliminating material constraints for nonlinearity with plasmonic metamaterials. *Nature Communications* 2015, **6**.

8. Yu N, Capasso F. Flat optics with designer metasurfaces. *Nat Mater* 2014, **13**(2)**:** 139-150.

9. Kildishev AV, Boltasseva A, Shalaev VM. Planar photonics with metasurfaces. *Science* 2013, **339**(6125)**:** 12320091-12320096.

10. Ni X, Kildishev AV, Shalaev VM. Metasurface holograms for visible light. *Nat Commun* 2013, **4**.

11. Chen WT, Yang KY, Wang CM, Huang YW, Sun G, Chiang ID, *et al.* High-efficiency broadband meta-hologram with polarization-controlled dual images. *Nano Letters* 2014, **14**(1)**:** 225-230.

12. Kauranen M, Zayats AV. Nonlinear plasmonics. *Nature Photonics* 2012, **6**(11)**:** 737-748.

13. Scalora M, Vincenti MA, de Ceglia D, Roppo V, Centini M, Akozbek N, *et al.* Second- and third-harmonic generation in metal-based structures. *Physical Review A* 2010, **82**(4)**:** 043828.

14. Ginzburg P, Krasavin AV, Wurtz GA, Zayats AV. Nonperturbative hydrodynamic model for multiple harmonics generation in metallic nanostructures. *ACS Photonics* 2015, **2**(1)**:** 8-13.

15. Klein MW, Enkrich C, Wegener M, Linden S. Second-Harmonic Generation from Magnetic Metamaterials. *Science* 2006, **313**(5786)**:** 502-504.

16. Belardini A, Larciprete MC, Centini M, Fazio E, Sibilia C, Chiappe D, *et al.* Circular dichroism in the optical second-harmonic emission of curved gold metal nanowires. *Physical Review Letters* 2011, **107**(25).

17. Sipe JE, So VCY, Fukui M, Stegeman GI. Analysis of second-harmonic generation at metal surfaces. *Physical Review B* 1980, **21**(10)**:** 4389-4402.

18. Forestiere C, Capretti A, Miano G. Surface integral method for second harmonic generation in metal nanoparticles including both local-surface and nonlocal-bulk sources. *J Opt Soc Am B* 2013, **30**(9)**:** 2355-2364.

19. Sadecka K, Toudert J, Surma HB, Pawlak DA. Temperature and atmosphere tunability of the nanoplasmonic resonance of a volumetric eutectic-based Bi2O3-Ag metamaterial. *Opt Express* 2015, **23**(15)**:** 19098-19111.

20. Xiong M, Jin X, Ye J. Strong plasmon coupling in self-assembled superparamagnetic nanoshell chains. *Nanoscale* 2016, **8**(9)**:** 4991-4999.

21. Turek VA, Francescato Y, Cadinu P, Crick CR, Elliott L, Chen Y, *et al.* Self-Assembled Spherical Supercluster Metamaterials from Nanoscale Building Blocks. *ACS Photonics* 2016, **3**(1)**:** 35-42.

22. Nasir ME, Peruch S, Vasilantonakis N, Wardley WP, Dickson W, Wurtz GA, *et al.* Tuning the effective plasma frequency of nanorod metamaterials from visible to telecom wavelengths. *Applied Physics Letters* 2015, **107**(12).

23. Mehrer H. *Diffusion in Solids : Fundamentals, Methods, Materials, Diffusion-controlled Processes*. Springer-Verlag Berlin and Heidelberg GmbH & Co. KG: Berlin, Germany, 2009.

24. Lejcek P. *Grain Boundary Segregation in Metals*. Springer Publishing Company, Incorporated, 2010.

25. Wachs AL, Miller T, Chiang TC. Evidence for germanium segregation on thin films of Ag on Ge(111). *Physical Review B* 1986, **33**(12)**:** 8870-8873.

26. Logeeswaran VJ, Kobayashi NP, Islam MS, Wu W, Chaturvedi P, Fang NX, *et al.* Ultrasmooth Silver Thin Films Deposited with a Germanium Nucleation Layer. *Nano Letters* 2009, **9**(1)**:** 178-182.

27. Chen W, Thoreson MD, Ishii S, Kildishev AV, Shalaev VM. Ultra-thin ultra-smooth and low-loss silver films on a germanium wetting layer. *Opt Express* 2010, **18**(5)**:** 5124-5134.

28. Stefaniuk T, Wróbel P, Górecka E, Szoplik T. Optimum deposition conditions of ultrasmooth silver nanolayers. *Nanoscale Res Lett* 2014, **9**(1)**:** 1-9.

29. Stefaniuk T, Wróbel P, Trautman P, Szoplik T. Ultrasmooth metal nanolayers for plasmonic applications: Surface roughness and specific resistivity. *Applied Optics* 2014(10)**:** B237-B241.

30. Wróbel P, Stefaniuk T, Trzcinski M, Wronkowska AA, Wronkowski A, Szoplik T. Ge wetting layer increases ohmic plasmon losses in ag film due to segregation. *ACS Appl Mater Interfaces* 2015, **7**(17)**:** 8999-9005.

31. Flötotto D, Wang ZM, Jeurgens LPH, Bischoff E, Mittemeijer EJ. Effect of adatom surface diffusivity on microstructure and intrinsic stress evolutions during Ag film growth. *J Appl Phys* 2012, **112**(4).

32. Zhang J, Fryauf DM, Garrett M, Logeeswaran VJ, Sawabe A, Islam MS, *et al.* Phenomenological Model of the Growth of Ultrasmooth Silver Thin Films Deposited with a Germanium Nucleation Layer. *Langmuir* 2015, **31**(28)**:** 7852-7859.

33. O'Donnell KA, Torre R, West CS. Observations of second-harmonic generation from randomly rough metal surfaces. *Physical Review B - Condensed Matter and Materials Physics* 1997, **55**(12)**:** 7985-7992.

34. Brown F, Parks RE, Sleeper AM. Nonlinear Optical Reflection from a Metallic Boundary. *Physical Review Letters* 1965, **14**(25)**:** 1029-1031.

35. Bloembergen N, Chang RK, Lee CH. Second-Harmonic Generation of Light in Reflection from Media with Inversion Symmetry. *Physical Review Letters* 1966, **16**(22)**:** 986-989.

Acknowledgments: This work has been supported, in part, by EPSRC (UK) and the ERC iPLASMM project (321268). A.Z. acknowledges support from the Royal Society and the Wolfson Foundation.

Author contributions: The experiments were conceived and designed by T.St, A.B, C.S, T.Sz and A.V.Z. The samples were fabricated by T.St. Linear optical characterization was performed by A.A.W and A.W. SHG measurements were carried by N.O. T.St. and A.B. SEM images were measured by T.St. Numerical modelling was performed by T.St. All authors contributed to writing of the manuscript and participated in data interpretation.

Competing financial interests: The authors declare that they have no competing interests.

Materials & Correspondence: Tomasz Stefaniuk tomasz.stefaniuk@kcl.ac.uk

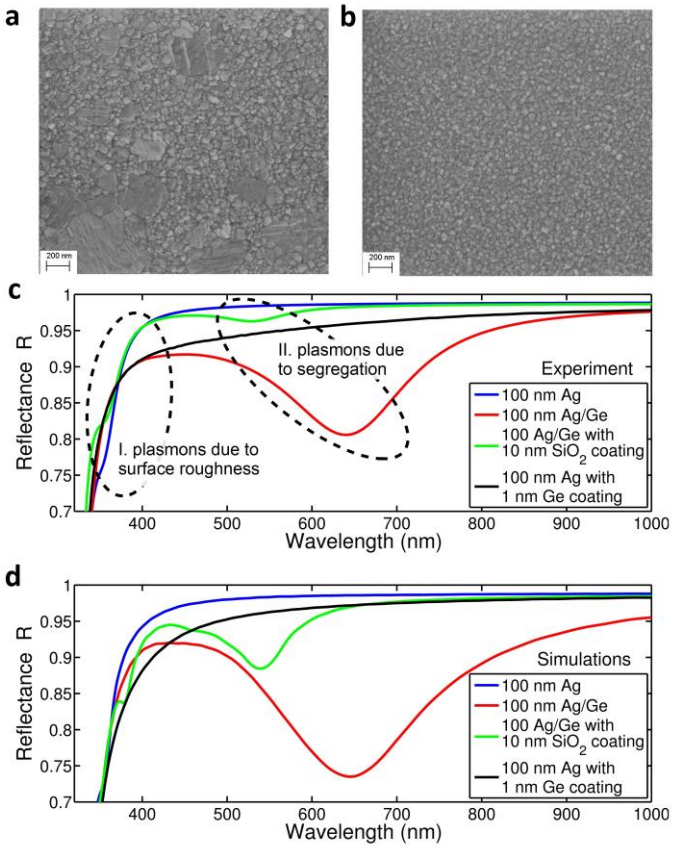

Figure 1 | Linear optical properties of Ag/Ge metasurface. SEM images of (A) Ag reference film and (B) Ag/Ge metasurface. (C) Experimentally measured and (D) numerically simulated reflectance spectra at normal incidence for different surface types.

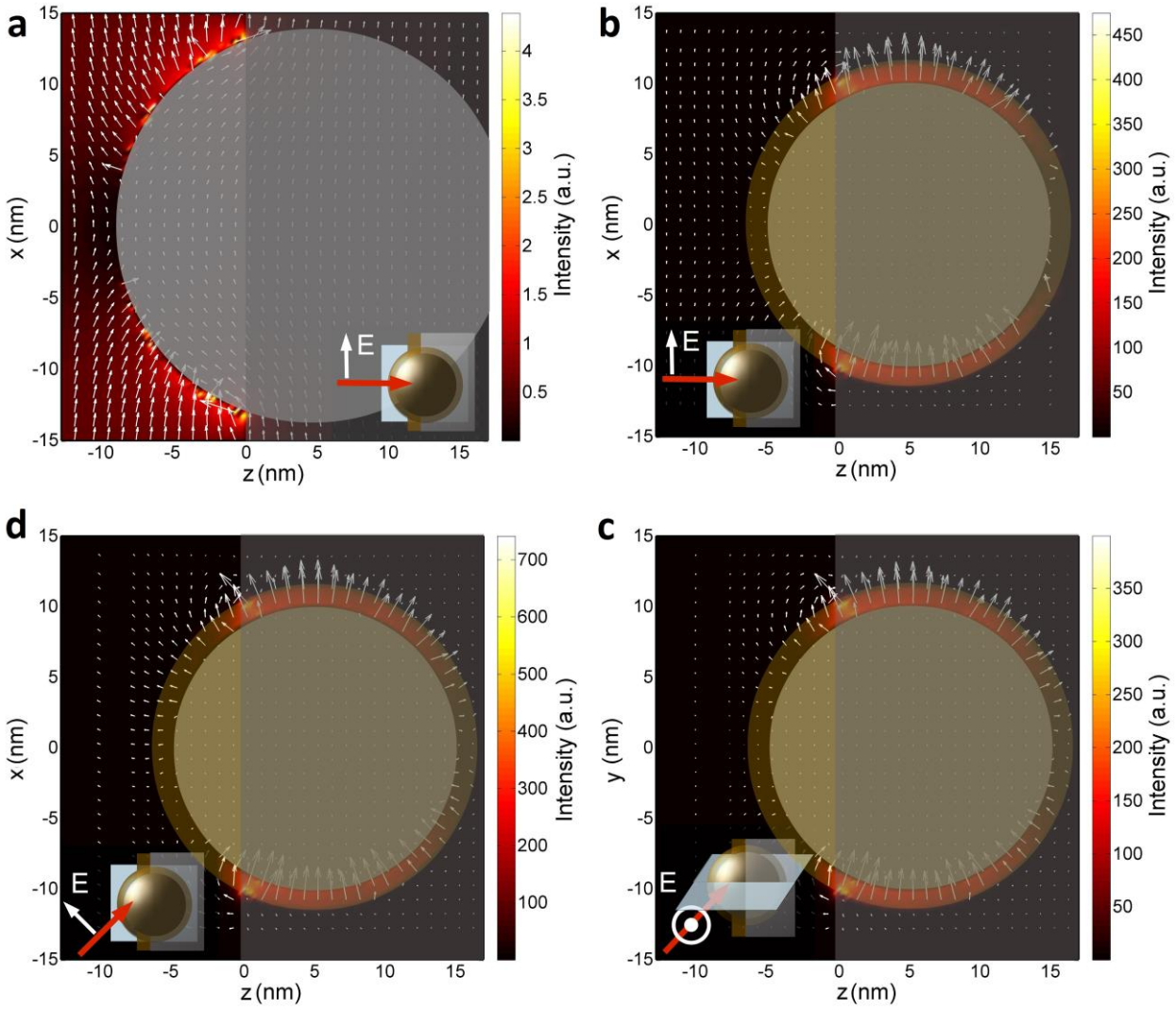

Figure 2 | LSP-induced intensity distributions at the metasurface. Intensity of the light (colour maps) and direction of the electric field (arrows) around the silver grains in (A) pure silver layer and (B-D) Ge-encapsulated Ag grains at a wavelength of 640 nm under (A, B) normal incidence and (C) p-polarized and (D) s-polarized illumination at 45^{o} incidence. Gray and brown circles depict electrically connected and electrically disconnected grains, respectively. Dark gray slab represents the Ag film volume. The insets show the orientation of the presented cross-sections.

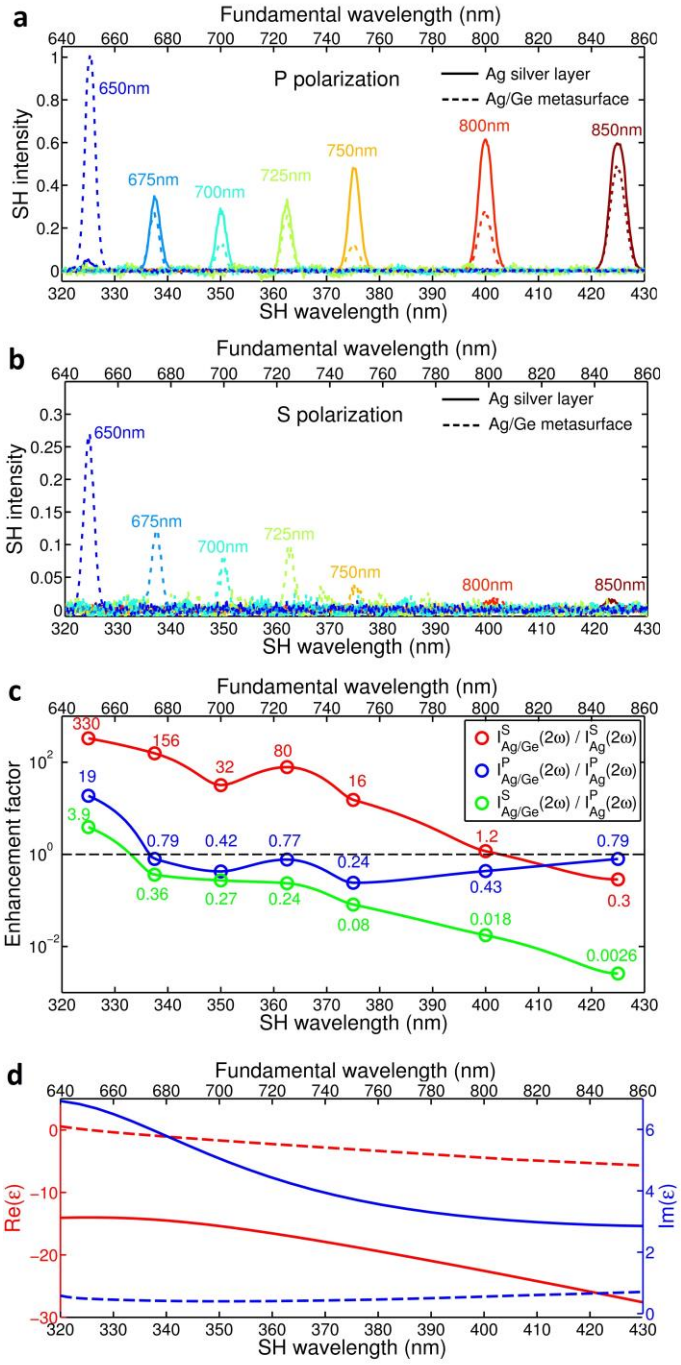

Figure 3 | Nonlinear properties of Ag/Ge metasurface. SH signal generated from Ag surface (solid lines) and Ag/Ge metasurface (dashed lines) for (A) p-polarized and (B) s-polarized incident light for different fundamental wavelengths. (C) Spectra of the SHG enhancement factor for different fundamental light polarizations. (D) Spectra of the real (red lines) and imaginary (blue lines) part of the effective permittivity of the Ag/Ge metasurface measured in 640-860 nm (solid lines) and 320-430 nm (dashed lines) wavelength ranges, corresponding to the studied fundamental and SH wavelengths.